International Journal of Environmental Science and Technology
https://doi.org/10.1007/s13762-021-03148-x

ORIGINAL PAPER

Essential role of B metal species in perovskite type catalyst structure and activity on toluene oxidation

R. Z. Yarbay Şahin[1,2,3] · M. Duplančić[4] · V. Tomašić[4] · J. H. Badia i Córcoles[3,5] · S. Kurajica[4]

Received: 3 September 2020 / Revised: 10 December 2020 / Accepted: 10 January 2021

Abstract

The perovskite type materials with transition metals are getting more attention especially as catalysts in total oxidation reaction. This work explores the B metal effect on the catalytic activity of $LaBO_3$ structured perovskites in total oxidation of toluene. The perovskite type oxides were obtained by Pechini method and characterized by X-ray diffraction, nitrogen adsorption/desorption isotherms, thermogravimetric analysis and differential scanning calorimetry, temperature-programmed reduction (H_2-TPR), Raman spectroscopy, Fourier transform infrared spectroscopy and particle size analysis. The results showed that $LaFeO_3$ catalyst contained a single orthorhombic $LaFeO_3$ phase, while $LaMnO_3$ contained $LaMn_2O_5$ species besides cubic $LaMnO_3$ phase. Both catalysts show very narrow distributions and average values of 55.59 µm and 51.43 µm for $LaMnO_3$ and $LaFeO_3$, respectively. With regard to the H_2-TPR profile for the $LaMnO_3$, Mn^{4+} to Mn^{3+} reduction and Mn^{3+} to Mn^{2+} reduction. Consequently, the redox performance of ABO_3 perovskites was found as mainly driven by the B-site transition-metal element character. According to the catalytic tests, the $LaMnO_3$ catalyst was more active for toluene oxidation than $LaFeO_3$ and achieved the lowest light-off temperatures. An excellent agreement between the experimental data and the proposed one-dimensional pseudo-homogeneous model was achieved and corresponding kinetic parameters (estimated rate constants, k, activation energies, E_A, and frequency factors, A_r) were estimated. Lower activation energy was estimated for $LaMnO_3$ catalyst (84 kJ mol^{-1} vs. 99 kJ mol^{-1} for $LaFeO_3$) confirming that $LaMnO_3$ catalyst was more active for toluene oxidation under reaction conditions presented in this paper.

Keywords Perovskite · B metal effect · Volatile organic chemicals oxidation · Toluene oxidation

Introduction

Attention to environmental pollutants due to its destructive effects on human health has grown significantly in recent years (Ensafi and Karimi-Maleh 2010; Karimi-Maleh et al. 2019).Pollution due to volatile organic compounds (VOCs) is becoming an increasingly serious problem worldwide since VOCs are a group of carbon comprising compounds that disappear at room temperature are described as carcinogenic, mutagenic and teratogenic to humankind (Liu et al. 2013; Pham and Lee 2015). VOCs are commonly present in both indoor and outdoor atmospheres since originating from natural emissions and anthropogenic sources such as motor vehicle exhausts and solvent usage. They also appear in biogas as a result of the anaerobic digestion of organic waste (Papurello et al. 2012). As a result of strict regulations related to VOC emissions, VOC removal from flue gas streams is a relevant research area. Toluene is a typical aromatic VOC (Wu et al. 2016) and the main approaches

Co-Author affiliations corrected.

Editorial responsibility: Fatih ŞEN.

✉ R. Z. Yarbay Şahin
Zerrin.yarbay@bilecik.edu.tr

1 Faculty of Engineering Chemical Engineering Department, Bilecik Seyh Edebali University, Bilecik, Turkey

2 Energy Technologies Application and Research Centre Bilecik, Bilecik Şeyh Edebali University, Bilecik, Turkey

3 Department of Advanced Materials for Energy, Catalonia Institute for Energy Research (IREC), Barcelona, Spain

4 Faculty of Chemical Engineering and Technology, University of Zagreb, Zagreb, Croatia

5 Departament d'Enginyeria Química i Química Analítica, Universitat de Barcelona, Barcelona, Spain

Published online: 27 January 2021

utilized in toluene removal from waste gases consist of adsorption, thermal incineration and catalytic oxidation (Liu et al. 2013).

Catalytic oxidation process is considered as an effective, economic and environmentally agreeable way of overcoming air pollution (Liu et al. 2013, 2017). Due to the complex molecular structure of VOCs, high temperatures above 673 K are required for their thermal incineration, but in the presence of a suitable catalyst the operating temperature can be significantly lower (Kim et al. 2017). The optimization of the desired catalytic material is a tough issue because of the great variety of VOCs and the VOC-containing mixtures complexity. Besides favouring low ignition temperatures, highly selective catalysts yielding with complete VOC breakdown to CO_2 and H_2O are desired. Also, long lifetime and thermal stability are expected as a characteristic of a good catalyst (Sihaib et al. 2017).

Noble metal-based catalysts, including Pd and/or Pt especially, have been intensively utilised in case of VOCs catalytic oxidation (Abdelouahab-Reddam et al. 2015; Huang et al. 2015). Nevertheless, these catalysts are known for being expensive as well as sensitive to the poisoning. As a result, transition-metal oxides are accepted as promising alternatives in terms of poisoning and cost advantages (Chen et al. 2014; Wang et al. 2017).

Perovskite type materials are famous for having flexible composition, superior thermal and hydrothermal stability, excellent redox properties and affordability in comparison with noble metal catalysts. Perovskite chemical formula ABO_3 allows modifying cations in either A- and/or B- position (Ding et al. 2017). In a classic structure, a lanthanide or alkaline-earth cation can be employed as A cation, while B cation which controls the catalytic activity is transition-metal element (Zhang et al. 2016; Li et al. 2017). Though perovskites are very well-known for their cubic structure, some other structures like rhombohedral and orthorhombic are probable synthesis outcomes. In cubic structure, coordination numbers of oxygen anions are 12 and 6 for A and B cation, respectively. (Zhang et al. 2016). A and O arrange a cubic nearby packing and B is exhibited in the octahedral voids in this structure. In order to obtain a perovskite crystal structure, the tolerance factor t which can be calculated from Eq. 1 below should meet the criteria including $0.8 < t < 1.0$, $r_A > 0.090$ nm, $r_B > 0.051$ nm (Tanaka and Misono 2001).

$$t = (r_A + r_{B)}/\sqrt{2}\left(r_B + r_O\right) \quad (1)$$

Perovskites and mesoporous perovskites are employed in the toluene catalytic oxidation (Wang et al. 2016; Zonouz et al. 2016; Sihaib et al. 2017). Wang et al. produced $LaMnO_3$ nano-catalysts for toluene oxidation and these catalysts were found to yield an activation energy (E_A) of 54.3 kJ mol^{-1} similar to catalysts containing noble metal (Wang et al. 2016). Sihaib et al. (Sihaib et al. 2017) investigated the activity of four manganese-based oxides including a $LaMnO_3$ prepared by sol–gel method; a Mn_2O_3 prepared by rapid method and octahedral molecular sieve (OMS-2) by two different preparation methods such as solid-state method (OMSs) and hydrothermal method (OMSh). As a result, the catalyst performance followed the order: OMSs > OMSh > Mn_2O_3 > $LaMnO_3$. A comparison of these catalysts revealed that OMS_S were more active even at low temperature starting to convert toluene at about 443 K, while in the case of Pd/Al_2O_3 conversion started at about 463 K (Sihaib et al. 2017). Zonouz et. al. (Zonouz et al. 2016) studied $La_{1-x}Ce_xMn_{1-y}Cu_yO_3$ as potential catalysts for toluene oxidation. According to hybrid artificial neural network-genetic algorithm method modelling and optimization results, the optimum composition of $La_{1-x}Ce_xMn_{1-y}Cu_yO_3$ was found at $x = 0.30$, $y = 0.52$ and calcination temperature of 898 K. The optimum conversion was obtained 513 K as 92.16% (Zonouz et al. 2016).

Though Mn-based perovskites are extensively investigated, iron-based perovskites are not often used in VOCs oxidation. On the other hands, some studies have been conducted concerning the application of mesoporous materials as good supports or templates for perovskite catalysts providing an increase in the specific surface area. Gao et. al. (2013) evaluated mesoporous $LaFeO_3$ catalysts for complete oxidation of CO and toluene. High catalytic activity obtained was attributed to the large surface area, high adsorbed oxygen concentration and low-temperature reducibility.

In this work, catalytic properties of two perovskite catalysts ($LaFeO_3$ and $LaMnO_3$) in the catalytic oxidation of toluene were investigated and compared. In our previous research, Mn and Fe proved to be effective components of a mixed metal oxide such as $MnFeO_x$ (Duplančić et al. 2017). Therefore, utilization of Mn and Fe as potential B cations in the perovskites was evaluated in this study.

Matherislas and methods

Materials

Lanthanum (III) nitrate hexahydrate (%99, ABCR), iron (III) nitrate nonahydrate (≥ 99.95%, Sigma-Aldrich), manganese (II) nitrate hexahydrate (For analysis, Acros) and citric acid monohydrate (Carlo Erba) were used in catalyst preparation step. All aqueous solutions were prepared with deionized water.

Catalyst preparation

The catalysts were prepared via Pechini (citrate) technique (Ghiasi and Malekzadeh 2014). Briefly, $La(NO_3)_3{\cdot}6H_2O$,

$Fe(NO_3)_3{\cdot}9H_2O$, $Mn(NO_3)_2{\cdot}3H_2O$ and citric acid monohydrate were used as precursors. All chemicals were of analytical grade. At first, calculated amounts of metal nitrate and citric acid were mixed until dissolved. Then, the homogeneous solution was evaporated at 338 K overnight. The swelled material was crushed in an agate mortar and put in a vacuum oven which was set to 353 K and 7000 Pa. The material was crushed every hour and maintained in the vacuum oven overnight. The oven was set to 373 K and 7000 Pa for a day. Finally, the solid obtained was calcinated at 1023 K with 10 K min^{-1} for 5 h under dry air in a quartz tubular reactor.

Catalyst characterization

Morphology of the catalysts was obtained from scanning electron microscope (SEM-Zeiss Auriga). XRD patterns of the catalysts were obtained with a Bruker D8 Advance XRD with CuKα radiation between 10° and 120° 2θ in a step scan mode with 0.02° steps and 0.6 s counting time. FT-IR spectra were recorded between 4000 and 700 cm^{-1} at a resolution of 4 cm^{-1} using PerkinElmer Spectrum One at room temperature. Textural parameters of the catalysts were determined by nitrogen adsorption/desorption isotherms on a TriStar II 3020 (micromeritics). Degasification of the samples was accomplished by first keeping them at 363 K for 1 h and then at 523 K for 4 h, at least, under nitrogen flow. Brunauer–Emmett–Teller (BET) method was used to calculate surface area in the relative pressure (P/P_0) range of 0.05–0.30 and Barrett–Joyner–Halenda (BJH) method was applied to the desorption isotherm to measure pore average size and volume. Temperature-programmed reduction (H_2-TPR) spectra were analysed on an AutoChem HP 2950 (Micromeritics) equipped with a thermal conductivity detector (TCD). About 90 mg of catalyst was used for each run. Prior to H_2-TPR, the sample was oxidized by treating it with 50 NmL min^{-1} of 10 vol% O_2/He, heated up from ambient temperature to 773 K, using a ramp of 10 K min^{-1} and with a hold of 30 min at that temperature. After the hold time, a flow of 50 NmL min^{-1} helium was used to flush the sample and it was cooled down to 308 K with a ramp of 10 K min^{-1}. Then, the sample was treated with 12 vol% H_2/Ar at a flow of 50 NmL min^{-1} in the temperature range from 308 to 1273 K, with a heating ramp of 5 K min^{-1} and a final hold time of 30 min. Thermogravimetric analysis with differential scanning calorimetry (TGA–DSC) of the samples was carried out on a Sensys Evo TG-DSC thermal analyser (Setaram). Fresh catalyst samples of 15–30 mg were heated up from ambient temperature to 1073 K, with a heating rate of 10 K min^{-1}, with a flow of 50 NmL min^{-1} of synthetic air. The same procedure was repeated but using an inert gas (i.e. argon) instead of synthetic air to elucidate the effect of temperature. Particle size distribution and average particle size of the catalysts were determined using a Mastersizer 2000 laser scattering unit using a LED type blue-lighted laser (466 nm beam wavelength) coupled with a Hydro 2000G dispersion unit (Malvern Instruments) with water as the dispersant agent.

Catalytic activity evaluation

Catalytic oxidation of toluene as a model VOC pollutant was carried out in an integral up-flow fixed-bed reactor operated in the temperature range of 373–573 K, at different space times and at atmospheric pressure. Scheme of the experimental system can be found elsewhere (Duplančić et al. 2018, 2020). The space times were studied by varying the total flow rate of the reaction mixture (23–138 cm^3 min^{-1}) at the fixed catalyst mass (0.05 g). Toluene oxidation was performed at a constant inlet toluene concentration in the reaction mixture (210 ppm toluene in nitrogen) and at a constant ratio of toluene/nitrogen and oxidant (air). The gas flow rates were regulated using two mass flow controllers (Brooks). The reactor temperature was regulated using a thermo-controller (TC208 Series) connected to a K-type thermocouple placed inside the reactor and using the heaters around the reactor. The reactor effluent was analysed by *on-line* gas chromatograph (Shimadzu GC-2014) equipped with a Carbowax 20 M column and with a flame ionization detector (FID). The activity of perovskites for toluene oxidation was evaluated by conversion of toluene at steady-state reaction conditions.

Fixed-bed reactor modelling

In order to describe the reactor steady-state behaviour under isothermal conditions and to compare activities of the prepared perovskite catalysts simple pseudo-homogeneous one-dimensional (1D) model of the fixed-bed reactor which neglects inter- and intra-phase diffusion was applied (Duplančić et al. 2018). Additional assumptions were considered, such as flat radial velocity profiles (plug flow of the fluid phase) and constant catalyst activity. Due to the large excess of oxidant, the toluene oxidation was described with first-order kinetic model. The corresponding model equations and numerical methods used for their solution may be found elsewhere (Sihaib et al. 2017; Duplančić et al. 2018).

Results and discussion

Physico–chemical properties of the prepared perovskites

XRD results

The crystal structure of the catalysts was analyzed via XRD analysis and results are given in Fig. 1. The presence of a single $LaFeO_3$ perovskite phase (orthorhombic; Pbnm space group, ICDD PDF #74-2203) was evident from the presence of diffraction peaks characteristic for this phase. Most prominent diffraction peaks are assigned to crystallographic planes as follows: 22.61°2θ (002) and (110), 32.17°2θ (112) and (220), 39.7°2θ (002) and (200), 46.16°2θ (004) and (220), 57.41°2θ (204) and (312), 67.3°2θ (040) and (224). No additional peaks revealing the presence of a second phase were apparent. On the other hands, $LaMnO_3$ catalyst showed $LaMnO_3$ cubic phase ($Pm\bar{3}m$space group, ICDD PDF #72-0840) and monoclinic $LaMn_2O_5$ (P21/c, ICDD PDF #52-1095). Most prominent diffraction peaks of LaMnO3 at 22.29, 31.12 and 32.31°2θ are assigned to (101), (002) and (200) planes, while most prominent diffraction peaks of LaMn2O5 at 28.24, 29.8, 35.05, 40.64, 46.15 and 57.85°2θ are assigned to (121), (211), (112), (212), (141) and (332) crystallographic planes. The RMn_2O_5 (R = rare-earth metal like La) family is attractive as having two different oxidation states for Mn, which are located at distinct oxygen atmospheres (Muñoz et al. 2005). Although the same preparation procedures applied, $LaFeO_3$ sample showed purity and far better crystallinity in comparison with $LaMnO_3$ sample. The remark on crystallinity is based on the comparison of diffraction maxima intensities and the appearance of amorphous hump on which peaks in sample $LaMnO_3$ are superimposed on. As can be seen the peak intensities in pattern of $LaFeO_3$ sample are 10 times larger than $LaMnO_3$ sample peak intensities. Such great difference for the samples analyzed under the same conditions makes claim on better crystallinity of sample $LaFeO_3$ plausible although no comparisons should be made without the addition of standards. Most of peaks in sample $LaMnO_3$ seem broad but which could be the consequence of small crystallite size but peaks are overlapped and inappropriate for Scherrer analysis.

Textural properties of the catalysts

Adsorption–desorption isotherms of N_2 at 77 K are shown in Fig. 2a. It can be seen that both curves correspond to type H3 hysteresis loops, which can be associated with non-rigid aggregates of plate-like particles with a macroporous pore network (Thommes et al. 2015). The metal type in B-position of the perovskite did not affect the total volume of N_2 adsorbed, which was quite similar for $LaFeO_3$ and $LaMnO_3$. On the other hands, the greatest contribution to pore volume can be attributed to the macroporous zone (> 50 nm) for both materials (Fig. 2b). Table 1 lists main textural properties of the materials. While $LaMnO_3$ catalyst showed a BET surface area of 3.72 m^2/g, $LaFeO_3$ catalyst had 4.45 m^2/g. As expected, very small BET surface areas were obtained,

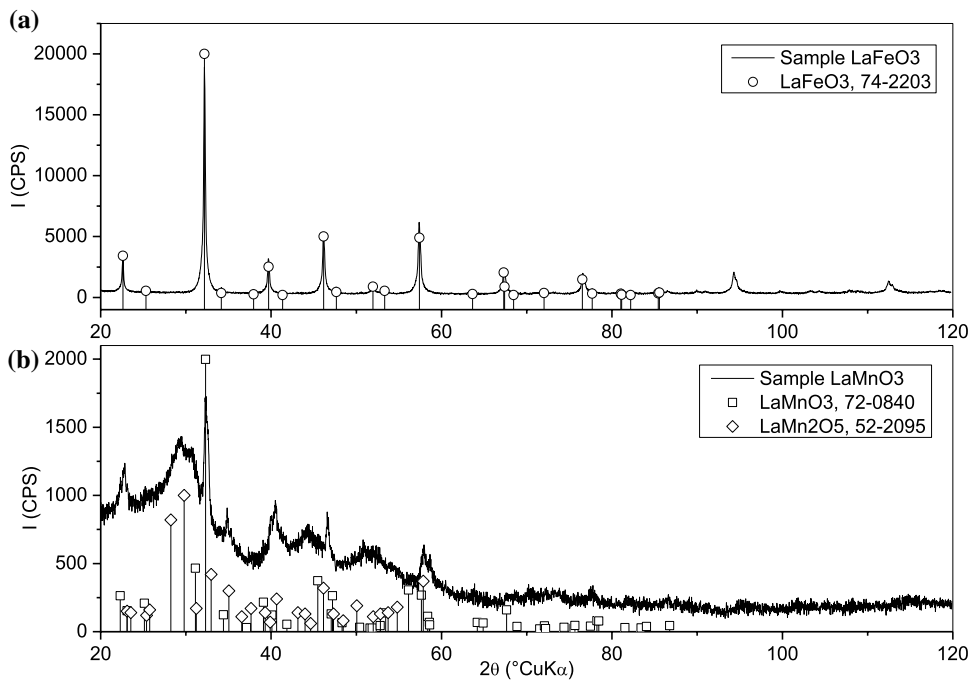

Fig. 1 XRD data for (**a**) $LaFeO_3$ and (**b**) $LaMnO_3$ catalysts

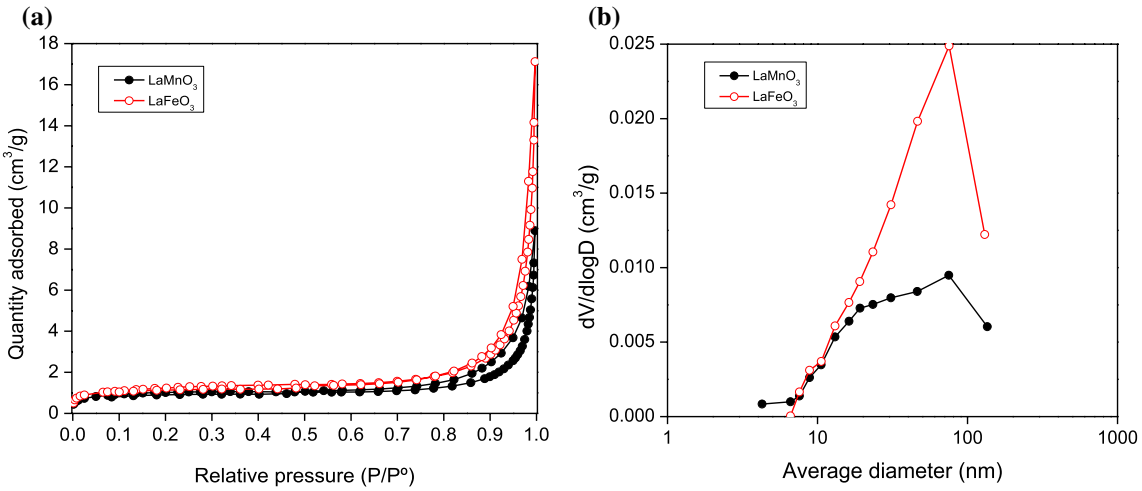

Fig. 2 N_2 adsorption–desorption isotherms (**a**) and BJH pore size distribution from N_2 desorption isotherm (**b**) for $LaMnO_3$ and $LaFeO_3$, respectively

Table 1 Textural properties of the prepared perovskite samples

Catalyst	BET surface area ($m^2\ g^{-1}$)	Pore volume ($cm^3\ g^{-1}$)	Average pore size (nm)
$LaFeO_3$	4.45	0.017	75.4
$LaMnO_3$	3.72	0.009	75.1

which is common for perovskite materials. Thus, additional effort should be made to develop nanostructured perovskite oxides and to increase the number of active sites per unit of their geometric area.

SEM results

The SEM micrographs of the catalysts are shown in Fig. 3. Two prepared samples exhibit the entirely different morphologies. The $LaFeO_3$ sample is consisted of particles of different sizes, from a few tens to a few hundred nanometers (Fig. 3a). Smaller particles exhibit some loose agglomeration

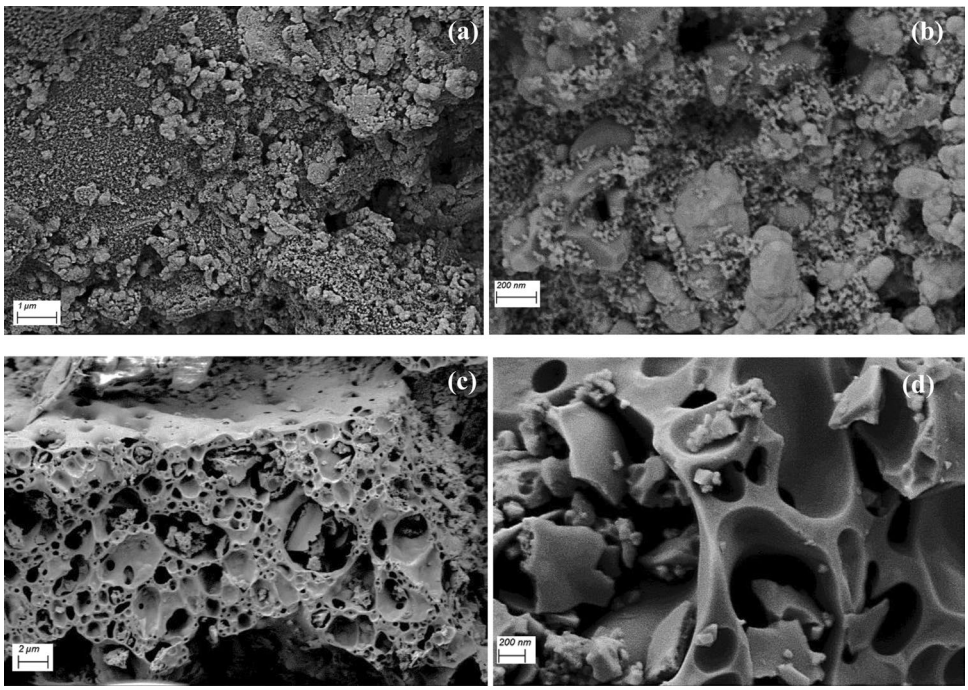

Fig. 3 SEM images of $LaFeO_3$ at (**a**) x10KX, (**b**) × 50KX and $LaMnO_3$ at (c) × 3KX and (d) × 30KX

but greater compact particles are void-free (Fig. 3b). On the other hands, the morphology of the $LaMnO_3$ sample could be described as sponge-like having voids partially filled with some crumbled particles (Fig. 3c). Such morphology is a consequence of gasses released in the course of synthesis and thermal treatment (Machin et al. 2008). The voids exhibit various dimensions, from submicron to few microns in diameter, while most of the crumbles, also exhibiting loose agglomeration, are in size range above 100 nm (Fig. 3d).

TGA–DSC results

Results of the TGA–DSC analysis (Figs. 4 and 5) under different gases flows (e.g. synthetic air and argon) show similar profiles for both perovskite catalysts. Mass losses of 15% and 27% were recorded for $LaFeO_3$ and $LaMnO_3$, respectively, when treated with synthetic air. When argon was used as the flow gas, mass losses were slightly reduced to 13% for $LaFeO_3$ and 21% for $LaMnO_3$. As seen in the figures, two regions can be distinguished in TGA curves, initial mass losses below 500–600 K can be related to water release and above 600 K oxygen losses would appear, which would be lower for Ar atmosphere (Santos 2010).

H_2-TPR results

Temperature-programmed reduction profiles of $LaFeO_3$ and $LaMnO_3$ samples are shown in Fig. 6. Two reduction steps can be observed for the $LaFeO_3$. First, there is a small peak at about 650 K, which would correspond to reduction of Fe^{3+} to Fe^{2+} and then a second reduction band, starting above 1000 K, which can be related to reduction of Fe^{2+} to Fe^0. These results are in agreement

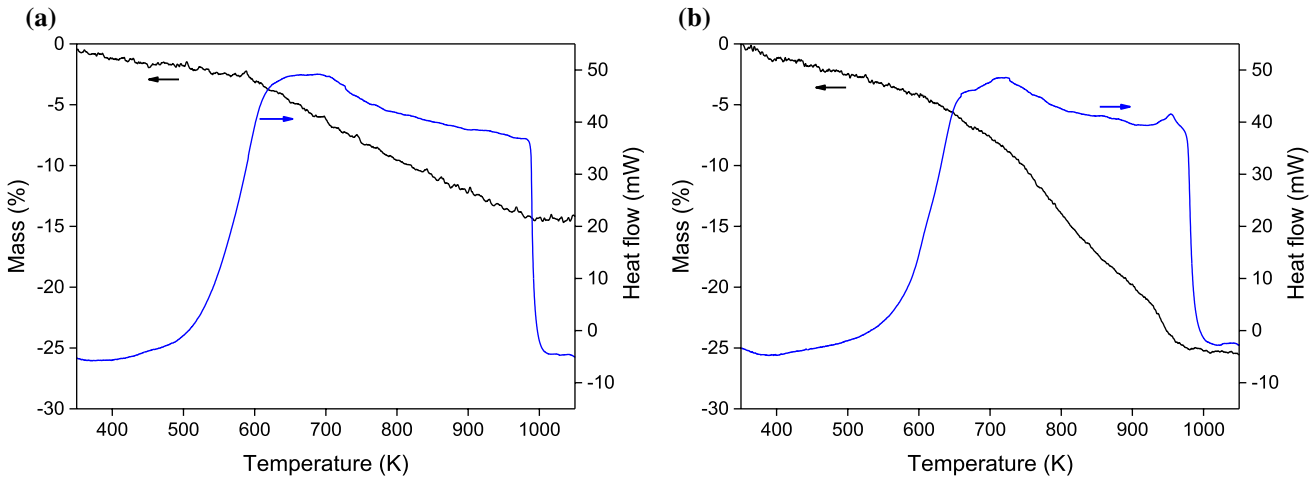

Fig. 4 TGA–DSC curve for $LaFeO_3$ (**a**) and for $LaMnO_3$ (**b**) catalysts under synthetic air flow

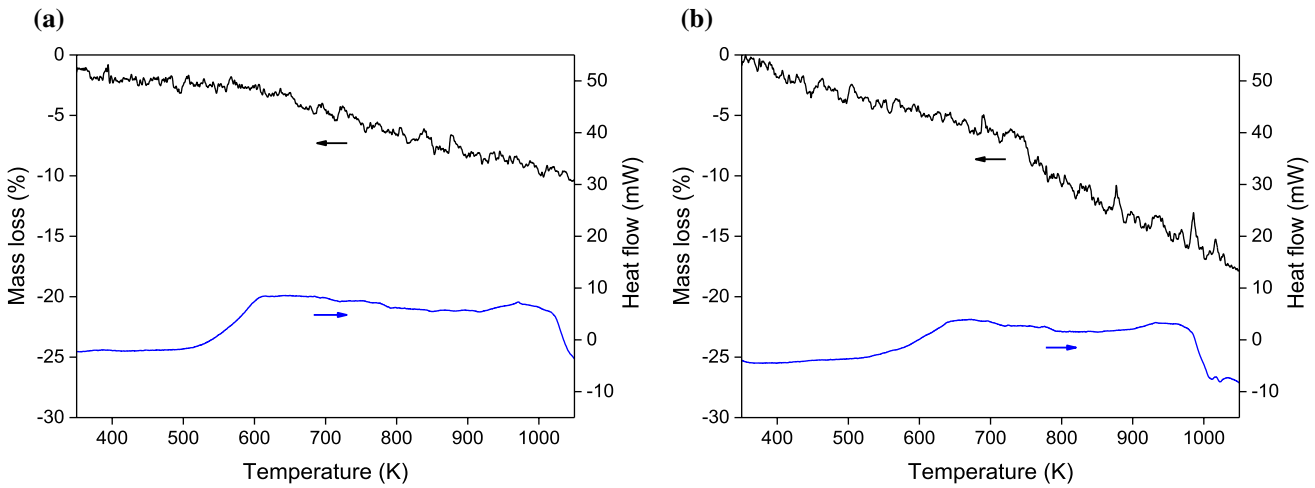

Fig. 5 TGA–DSC curve for $LaFeO_3$ (**a**) and for $LaMnO_3$ (**b**) catalysts under Ar flow

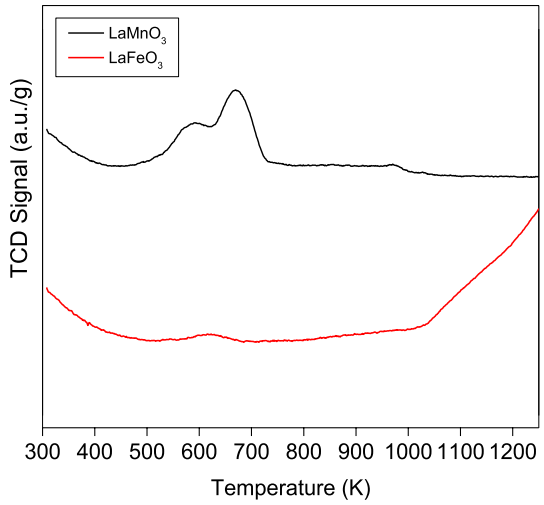

Fig. 6 Temperature-programmed reduction profiles for $LaMnO_3$ and $LaFeO_3$

with the literature (Heidinger et al. 2019). With regards to the H_2-TPR profile for the $LaMnO_3$ sample, first peak appears in the temperature range between 500 and 700 K and a second one, with a significantly smaller intensity, centered at around 950 K. The first one is typically related to Mn^{4+} to Mn^{3+} reduction and the second peaks show the reduction of Mn^{3+} to Mn^{2+} (Ansari et al. 2019). The shoulder in the first peak of the $LaMnO_3$ sample indicates different Mn species in the perovskite. According to the literature, the redox performance of ABO_3 perovskites is mainly driven by the B-site transition-metal element character and the role of the rare-earth ions in the A-site (such as La) is accepted as secondary (Nitadori et al. 1988; Zhu et al. 2015).

Raman results

Raman spectroscopy is a powerful technique for the phase structural analysis. Compared to XRD, its excitation energy which is less penetrating than X-ray makes it more surface-sensitive (Feng et al. 2011). Figure 7 shows Raman spectra of $LaFeO_3$ and $LaMnO_3$. Similar results were observed in the previous studies approving the formation of the phases in crystal systems (Palimar et al. 2016). Raman spectra showed a strong broadening of bands for $LaMnO_3$ compared to $LaFeO_3$. The vibrational modes frequencies found can be classified as follows: (1) vibrations of A-site cations (below 200 cm^{-1}), (2) octahedral bending modes (250–450 cm^{-1}) and (3) octahedral stretching modes (500–600 cm^{-1}) (Runka and Berkowski 2012; Palimar et al. 2016). In addition to the perfect $LaFeO_3$ crystal structure verified by XRD analysis, additional information was obtained based on Raman spectra, i.e. three clear bands at about 764, 941 and 1477 cm^{-1}. The band at 764 cm^{-1} indicated to Fe–O and La–O stretch vibrations. Broad bands with high intensity were detected at ~ 941 and ~ 1477 cm^{-1}. These bands can be explained as second-order scattering of IR-active longitudinal optic phonon modes (Nandi et al. 2018).

The perovskite which has excellent cubic structure does not keep Raman active phonons due to all the five atoms of the unit cell reside in centrosymmetrical positions. Raman active phonons can be shown in (a) mismatch of the ions ionic radii in the unit cell and the (b) Jahn–Teller effect related to the Mn^{3+} ions ensure origin to the orthorhombic (Pnma) and the rhombohedral (R-3c) structures (Varshney and Shaikh 2014). The broad bands between 375 and 920 cm^{-1} in the Raman spectra of orthorhombic $LaMnO_3$ link to lattice vibrations initiated by the dynamic Jahn–Teller effect and the existence of small polarons round the Mn^{3+} sites.

The Raman results indicate that the relationship between the Jahn–Teller distortion and the phonon

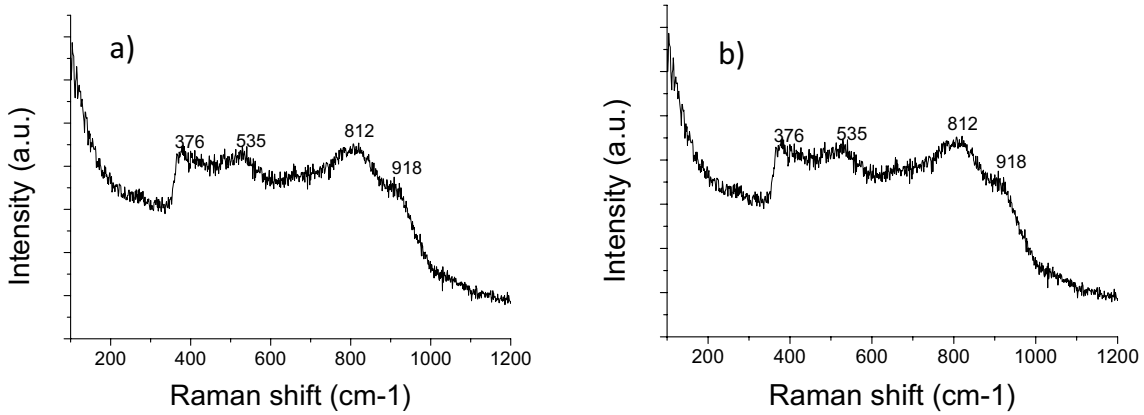

Fig. 7 Raman spectra of **a** $LaFeO_3$ and **b** $LaMnO_3$ catalyst

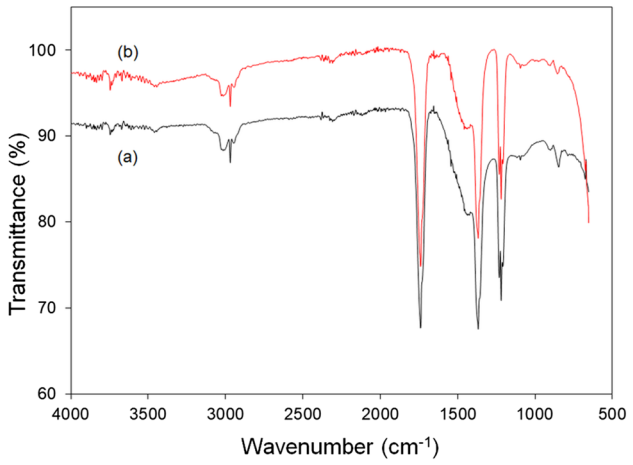

Fig. 8 FT-IR spectra of $LaMnO_3$ (a) before and (b) after the catalytic oxidation of toluene

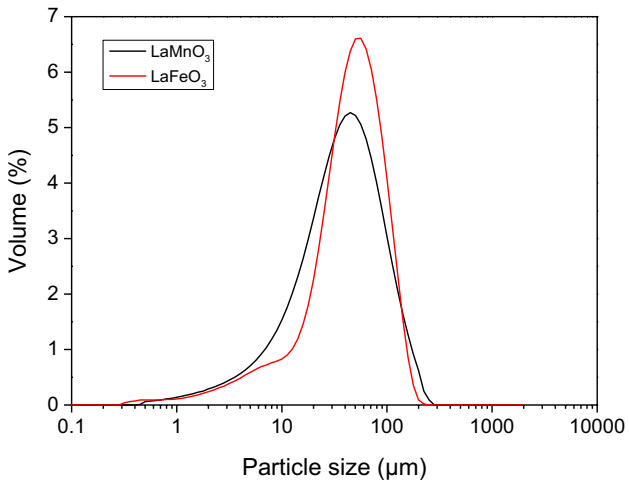

Fig. 9 Average particle size for $LaMnO_3$ and $LaFeO_3$

intensity is acceptable over a large temperature range. But, especially the peaks are apparent at and above the phase transition temperature as Mn–O octahedra are consistent according to diffraction. The atomic movements in Fig. 8 are consistent with the results conducted by Martin-Carron et al. There is a structural phase transition at about 800 K to a quasicubic structure and, considering that a cubic perovskite has no Raman modes permitted, the Raman peaks are expected to eliminate at or close the phase transition temperature (Martín-Carrón and De Andrés 2001).

FT-IR results

The FT-IR analysis was employed to investigate the changes in the chemical composition of the $LaMnO_3$ catalyst before and after toluene oxidation. The FT-IR spectra given in Fig. 8 revealed that there was no significant adsorption of the reactants or possible reaction intermediates on the surface of the $LaMnO_3$ during the toluene oxidation. While the peak at 1380 cm^{-1} (M–O rocking in plane) indicated the presence of metal-oxide group, the peaks at 1740 cm^{-1} (C=O or M-H stretching) and at 1210 cm^{-1} (C–O stretching) implied some carbon-containing molecules.

Particle size analysis results

Particle size distributions of the two catalysts, as determined by laser scattering, are shown in Fig. 9. Both catalysts show very narrow distributions and average values of 55.588 μm and 51.432 μm for $LaMnO_3$ and $LaFeO_3$, respectively. Main results, expressed as the average of four separate runs, are listed in Table 2.

Catalytic experiments

Oxidation of toluene was used as a model reaction to compare the activity of the prepared perovskite catalysts. The influence of the reaction temperature and total flow rate of the reaction mixture on the conversion of toluene over $LaFeO_3$ and $LaMnO_3$ catalysts is shown in Fig. 10. With the increase in temperature, the conversion of toluene increased and reached a maximum value depending on the operating conditions, i.e. depending on the space time. As expected, at larger space times (i.e. at lower total flow rate of the reaction mixture), the maximum conversion of toluene was achieved at lower temperatures. The $LaMnO_3$ perovskite was more active catalyst for toluene oxidation than $LaFeO_3$ and achieved lower T_{10}, T_{50} and T_{90} temperatures, e.g. temperatures corresponding to the 10%, 50% and 90% of toluene conversion (Fig. 11, Table 3), regardless of the total flow rate of the reaction mixture. Data for the commercial Pt-Al_2O_3 were taken from (Duplancic 2018).

The observed curves with characteristic S-shape in Fig. 10 represent dependence of toluene conversion on reaction temperature, which indicates that toluene conversion increases sharply with increasing temperature until the inflection point is reached, followed by a slower increase in toluene conversion with further increase in temperature.

Table 2 Particle size distribution results

	$LaFeO_3$	$LaMnO_3$
Average particle size (μm)	55.588	51.432
Uniformity	0.588	0.781
< 10 vol% (μm)	11.594	9.065
< 50 vol% (μm)	48.951	39.878
< 90 vol% (μm)	107.302	109.714

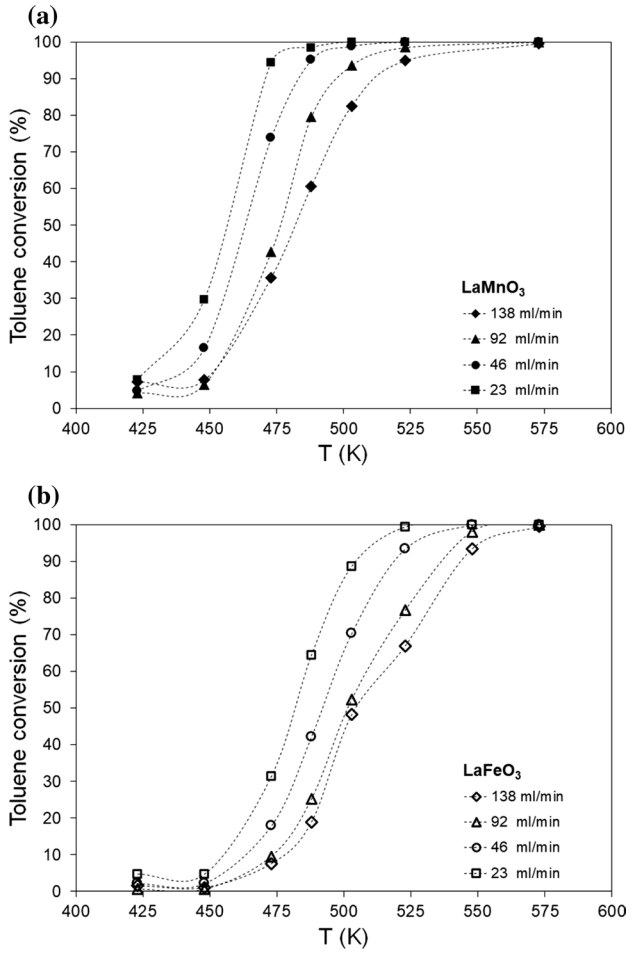

Fig. 10 Catalytic performance of (**a**) $LaMnO_3$ and (**b**) $LaFeO_3$ at different temperatures and total flow rates of reaction mixture

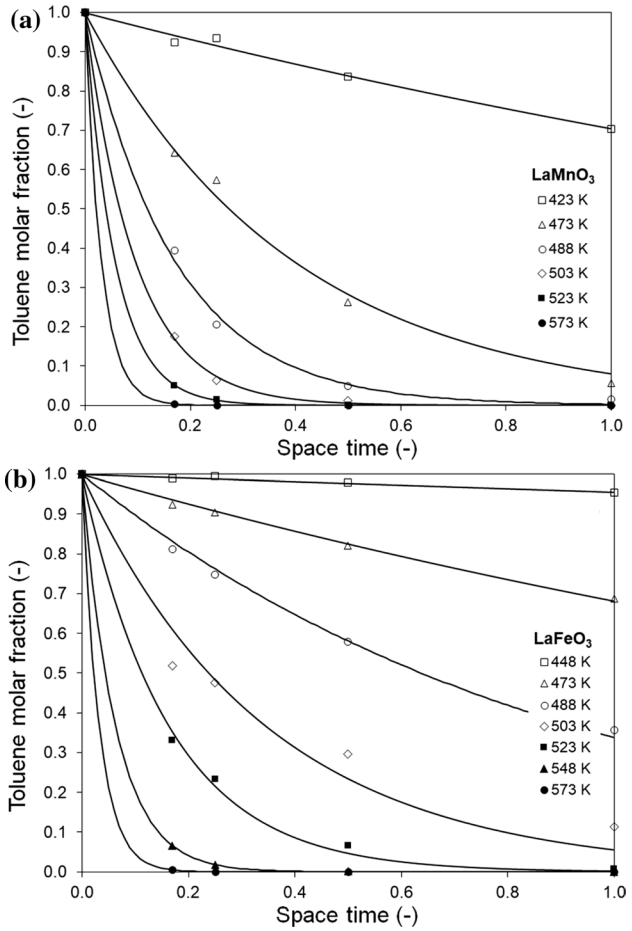

Fig. 11 Comparison between experimental data (points) and values predicted by the 1D pseudo-homogeneous model (lines) for (**a**) $LaMnO_3$ and (**b**) $LaFeO_3$ catalyst

This form of curve is well-known and characteristic for the exothermal reactions of oxidation, which results in the rapid release of the reaction heat and transition from the kinetic to the diffusion region during the reaction path. Extremely exothermic reactions are often present in industrial practice and therefore a great care must be taken during the reactor design, because of the risk connected with this kind of reactions. Based on the shape of the S-curve, it is possible to get an additional insight into the kinetic properties of the catalyst and to draw conclusions about the reaction order as well as about the influence of both the intra-phase and inter-phase diffusion on the overall reaction rate. From the shape of the curves obtained on the catalysts employed in this study, it seems that toluene oxidation is a first-order reaction (Duprat 2002).

Characteristic values T_{10}, T_{50} and T_{90}, e.g. temperatures corresponding to the 10%, 50% and 90% of toluene conversion over $LaMnO_3$ and $LaFeO_3$ at different total flow rates of the reaction mixture are shown in Table 3. For comparison purposes, Table 3 also contains T_{10}, T_{50} and T_{90} for the commercial Pt-Al_2O_3 catalyst that served as a benchmark. The characteristic value of T_{50} for the $LaMnO_3$ catalyst is 456–481 K, while for $LaFeO_3$, it is between 481–506 K,

Table 3 Comparison of the activities of perovskite catalysts and commercial Pt-Al_2O_3 catalyst based on T_{10}, T_{50} and T_{90} at different total flow rates of the reaction mixture

v_0, $cm^3\ min^{-1}$		138	92	46	23
$LaFeO_3$	T_{10}, K	477	474	460	453
	T_{50}, K	506	502	492	481
	T_{90}, K	545	540	520	505
$LaMnO_3$	T_{10}, K	450	450	435	425
	T_{50}, K	481	477	462	456
	T_{90}, K	515	500	485	471
Pt-Al_2O_3[a]	T_{10}, K	397	393	384	378
	T_{50}, K	411	404	396	387
	T_{90}, K	423	415	403	393

[a]Data for the commercial Pt-Al_2O_3 were taken from (Duplancic 2018)

depending on the total flow of the reaction mixture (or space time). Comparing the T_{90} values obtained with perovskite catalysts and commercial Pt-Al_2O_3, it can be seen that $LaMnO_3$ achieves 90% conversion at temperatures that are 78–92 K (depending on the total flow rate) higher than that for Pt-Al_2O_3, while in the case of $LaFeO_3$, these differences are even more pronounced (112–125 K, depending on total flow rate). These temperature differences indicate that perovskite catalysts have poorer catalytic properties in the catalytic oxidation of toluene in comparison to the commercial Pt-Al_2O_3 catalyst. However, a possible strategy to further improve activity of perovskite catalyst for toluene oxidation involves incorporating or impregnating a precious metal such as Pt or Pd into its structure, as shown by Giebeler et al. (Giebeler et al. 2007).

The higher activity of the $LaMnO_3$ compared to $LaFeO_3$ origins from different Mn species as described previously based on the characterization results, i.e. XRD (Fig. 1), H_2-TPR (Fig. 6) and Raman analysis (Fig. 7). Therefore, the results obtained by comparing the catalytic activity of two perovskites for toluene oxidation are consistent with the results of their characterization.

Although the presence of highly dispersed oxide phases with reduced crystallinity and medium crystallite size is not desirable, the presence of $LaMn_2O_5$ on the surface of $LaMnO_3$ crystallites leads to the improved catalyst activity. In addition, the co-presence of $LaMn_2O_5$ provides a synergistic effect, i.e. improves the reducibility of the catalyst, promotes the formation of abundant lattice oxygen and thus improves catalytic activity for the oxidation of toluene. Based on the results of the particle size distribution (Fig. 9, Table 2) it is confirmed that the oxidation of toluene is a structure-sensitive reaction, like the oxidation of benzene (Garcia et al. 2014).

Pseudo-homogeneous one-dimensional (1D) model of the fixed-bed reactor

Evaluations of experimental data and theoretical values predicted by the applied mathematical models are graphically shown in Fig. 11a for the $LaMnO_3$ and in Fig. 11b for the $LaFeO_3$ catalyst. A very good agreement between simulation and experimental data was attained, demonstrating that applied mathematical model produced acceptable outcomes for the catalytic oxidation of toluene in the described experimental settings. The values of the estimated rate constants, k and the root-mean-square deviations, SD at different temperatures are assumed in Table 4 for both catalysts. The activation energies, E_A and frequency factors, A_r calculated from the Arrhenius plots (not shown here) are also reported in Table 4. The obtained E_A values are 83.71 kJ mol^{-1} and 99.16 kJ mol^{-1} for the $LaMnO_3$ and $LaFeO_3$, respectively. Similar, but higher values of activation energies ranging from 126 to 164 kJ mol^{-1} are reported for $LaBO_3$ (B: Mn, Fe) perovskites prepared using a three-step reactive grinding process (Heidinger et al. 2019). Obviously, the perovskite with a lower E_A value exhibits the better catalytic performance for toluene oxidation.

Table 4 Estimated rate constants at different temperatures for the $LaMnO_3$ and $LaFeO_3$ catalyst

	T (K)	k (min^{-1})	SD × 10^3
$LaMnO_3$	423	47.17	12.04
	448	171.05	5.42
	473	1232.16	10.68
	488	2858.14	7.71
	503	5089.61	2.57
	523	8489.34	0.46
	573	15,856.69	0.06
	$A_r = 1.52 \times 10^{12}$ min^{-1}; $E_A = 83.71$ kJ mol^{-1}		
$LaFeO_3$	423	20.13	2.01
	448	22.43	1.25
	473	185.80	3.07
	488	524.35	6.22
	503	1399.89	25.34
	523	2951.50	6.8
	548	7704.09	0.35
	573	14,997.18	0.12
	$A_r = 1.98 \times 10^{13}$ min^{-1}; $E_A = 99.16$ kJ mol^{-1}		

Conclusions

The study deals with catalytic oxidation of toluene over $LaMnO_3$ and $LaFeO_3$ perovskite type catalysts prepared by Pechini method. It is observed that $LaMnO_3$ displays better catalytic activity for toluene oxidation which is attributed to its physico–chemical properties determined by different instrumental techniques. According to the obtained results, $LaMnO_3$ contains different Mn species and oxygen vacancies which are probably critical in maintaining the high activity and stability. Different Mn species are confirmed by XRD and H_2-TPR analysis, while oxygen vacancies that outcomes from the broadening of vibrational bands are confirmed by Raman analysis. The Raman spectrum of $LaMnO_3$ also showed the contribution of additional phase, such as monoclinic $LaMn_2O_5$. The coexistence of $LaMn_2O_5$ and $LaMnO_3$ causes a synergistic action, which results in better reducibility of perovskite catalyst, the formation of active lattice oxygen and thus improved the activity of the catalyst.

A good agreement of the experimentally observed results with the values predicted by the proposed one-dimensional (1D) pseudo-homogeneous model of the fixed bed reactor is achieved, indicating that the proposed

model can be successfully applied to describe the experimental system. The calculated apparent activation energies for toluene oxidation on the $LaMnO_3$ and $LaFeO_3$ catalyst were 84 kJ mol^{-1} and 99 kJ mol^{-1}, respectively. The lowest apparent activation energy of $LaMnO_3$ is in good agreement with its better catalytic behaviour for toluene oxidation under conditions employed in this study. Finally, based on the obtained results, it follows that $LaMnO_3$ is a potential catalyst for the catalytic oxidation of volatile organic compounds in real systems.

Acknowledgements Rahmiye Zerrin Yarbay Şahin appreciated the "Scientific and Technological Research Council of Turkey (TUBITAK) BIDEB-2219 International Postdoctoral Research Fellowship Programme" for financial support. This work is partially supported by the Croatian Science Foundation under the project In-PhotoCat (IP-2018-01-8669). The authors also thank to Marc Nuñez Eroles for Raman Measurements and Prof. Dr. Albert Tarancon for his support to this work.

Compliance with ethical standards

Conflict of interest The authors declare that they have no known competing financial interests or personal relationships that could have appeared to influence the work reported in this paper.

References

Abdelouahab-Reddam Z, El MR, Coloma F, Sepúlveda-Escribano A (2015) Platinum supported on highly-dispersed ceria on activated carbon for the total oxidation of VOCs. Appl Catal A Gen. https://doi.org/10.1016/j.apcata.2015.01.026

Ansari AA, Ahmad N, Alam M et al (2019) Physico-chemical properties and catalytic activity of the sol-gel prepared Ce-ion doped LaMnO3 perovskites. Sci Rep. https://doi.org/10.1038/s41598-019-44118-1

Chen H, Yan Y, Shao Y, Zhang H (2014) Catalytic activity and stability of porous Co–Cu–Mn mixed oxide modified microfibrous-structured ZSM-5 membrane/PSSF catalyst for VOCs oxidation. RSC Adv. https://doi.org/10.1039/c4ra08769k

Ding Y, Wang S, Zhang L et al (2017) A facile method to promote LaMnO3 perovskite catalyst for combustion of methane. Catal Commun. https://doi.org/10.1016/j.catcom.2017.04.022

Duplančić M, Tomašić V, Kurajica S et al (2017) A comparative study of toluene oxidation on different metal oxides. Chem Eng Trans. https://doi.org/10.3303/CET1757149

Duplančić M, Tomašić V, Gomzi Z (2018) Catalytic oxidation of toluene: comparative study over powder and monolithic manganese-nickel mixed oxide catalysts. Environ Technol (UK). https://doi.org/10.1080/09593330.2017.1346713

Duplančić M, Gomzi V, Pintar A et al (2020) Experimental and theoretical (ReaxFF) study of manganese-based catalysts for low-temperature toluene oxidation. Ceram Int. https://doi.org/10.1016/j.ceramint.2020.09.147

Duplancic M (2018) Catalytic oxidation of toluene in a metal monolith reactor. PhD dissertation, University of Zagreb, Zagreb

Duprat F (2002) Light-off curve of catalytic reaction and kinetics. Chem Eng Sci. https://doi.org/10.1016/S0009-2509(01)00409-2

Ensafi AA, Karimi-Maleh H (2010) Ferrocenedicarboxylic acid modified multiwall carbon nanotubes paste electrode for voltammetric determination of sulfite. Int J Electrochem Sci 5(3):392–406

Feng J, Liu T, Xu Y et al (2011) Effects of PVA content on the synthesis of LaFeO3 via sol-gel route. Ceram Int. https://doi.org/10.1016/j.ceramint.2010.11.045

Gao B, Deng J, Liu Y et al (2013) Mesoporous LaFeO3 catalysts for the oxidation of toluene and carbon monoxide. Cuihua Xuebao/Chinese J Catal. https://doi.org/10.1016/s1872-2067(12)60689-5

Garcia T, Solsona B, Taylor SH (2014) Chapter 3 The catalytic oxidation of hydrocarbon volatile, pp 51–90

Ghiasi M, Malekzadeh A (2014) Solar photocatalytic degradation of methyl orange over La 0.7Sr0.3MnO3 nano-perovskite. Sep Purif Technol. https://doi.org/10.1016/j.seppur.2014.07.022

Giebeler L, Kießling D, Wendt G (2007) LaMnO3 perovskite supported noble metal catalysts for the total oxidation of methane. Chem Eng Technol. https://doi.org/10.1002/ceat.200600306

Heidinger B, Royer S, Alamdari H et al (2019) Reactive grinding synthesis of LaBo3 (B: Mn, Fe) perovskite; properties for toluene total oxidation. Catalysts. https://doi.org/10.3390/catal9080633

Huang H, Xu Y, Feng Q, Leung DYC (2015) Low temperature catalytic oxidation of volatile organic compounds: a review. Catal. Sci. Technol 5(5):2649–2669

Karimi-Maleh H, Fakude CT, Mabuba N et al (2019) The determination of 2-phenylphenol in the presence of 4-chlorophenol using nano-Fe3O4/ionic liquid paste electrode as an electrochemical sensor. J Colloid Interface Sci. https://doi.org/10.1016/j.jcis.2019.07.047

Kim IH, Park EJ, Park CH et al (2017) Activity of catalysts consisting of Fe2O3 nanoparticles decorating entire internal structure of mesoporous Al2O3 bead for toluene total oxidation. Catal Today. https://doi.org/10.1016/j.cattod.2017.03.023

Li P, Zhang R, Liu N, Royer S (2017) Efficiency of Cu and Pd substitution in Fe-based perovskites to promote N2 formation during NH3 selective catalytic oxidation (NH3-SCO). Appl Catal B Environ. https://doi.org/10.1016/j.apcatb.2016.10.021

Liu ZS, Chen JY, Peng YH (2013) Activated carbon fibers impregnated with Pd and Pt catalysts for toluene removal. J Hazard Mater. https://doi.org/10.1016/j.jhazmat.2013.04.007

Liu Y, Guo Y, Liu Y et al (2017) SnO 2 nano-rods promoted by In, Cr and Al cations for toluene total oxidation: the impact of oxygen property and surface acidity on the catalytic activity. Appl Surf Sci. https://doi.org/10.1016/j.apsusc.2017.05.146

Machin NE, Karakaya C, Celepci A (2008) Catalytic combustion of methane on La-, Ce-, and Co-based mixed oxides. Energy Fuels. https://doi.org/10.1021/ef8000983

Martín-Carrón L, De Andrés A (2001) Melting of the cooperative Jahn–Teller distortion in LaMnO3 single crystal studied by Raman spectroscopy. Eur Phys J B. https://doi.org/10.1007/PL00011129

Muñoz A, Alonso JA, Casais MT et al (2005) A study of the magnetic structure of LaMn2O5 from neutron powder diffraction data. Eur J Inorg Chem. https://doi.org/10.1002/ejic.200400548

Nandi S, Blanck D, Carlier T, et al (2018) LaFeO3 thin films as relevant models for the surface investigation of 3-way catalysts. In: Surface and interface analysis

Nitadori T, Ichiki T, Misono M (1988) Catalytic properties of perovskite-type mixed oxides (ABO 3) consisting of rare earth and 3d transition metals. In: The Roles of the A- and B-Site Ions. Bull Chem Soc Jpn. https://doi.org/10.1246/bcsj.61.621

Palimar S, Kaushik SD, Siruguri V et al (2016) Investigation of Ca substitution on the gas sensing potential of LaFeO3 nanoparticles towards low concentration SO2 gas. Dalt Trans. https://doi.org/10.1039/c6dt01819j

Papurello D, Soukoulis C, Schuhfried E et al (2012) Monitoring of volatile compound emissions during dry anaerobic digestion of the organic fraction of municipal solid waste by proton transfer

reaction time-of-flight mass spectrometry. Bioresour Technol 126:254–265

Pham TD, Lee BK (2015) Novel adsorption and photocatalytic oxidation for removal of gaseous toluene by V-doped TiO2/PU under visible light. J Hazard Mater. https://doi.org/10.1016/j.jhazmat.2015.07.048

Runka T, Berkowski M (2012) Perovskite La 1-xSr xGa 1-yMn yO 3 solid solution crystals: Raman spectroscopy characterization. J Mater Sci 47:5393–5401. https://doi.org/10.1007/s10853-012-6422-2

Santos VP da CO (2010) Catalytic oxidation of volatile organic compounds in industrial off-gases. PhD dissertation, University of Porto, Portugal

Sihaib Z, Puleo F, Garcia-Vargas JM et al (2017) Manganese oxide-based catalysts for toluene oxidation. Appl Catal B Environ. https://doi.org/10.1016/j.apcatb.2017.03.042

Tanaka H, Misono M (2001) Advances in designing perovskite catalysts. Curr Opin Solid State Mater Sci. https://doi.org/10.1016/S1359-0286(01)00035-3

Thommes M, Kaneko K, Neimark AV et al (2015) Physisorption of gases, with special reference to the evaluation of surface area and pore size distribution (IUPAC Technical Report). Pure Appl Chem. https://doi.org/10.1515/pac-2014-1117

Varshney D, Shaikh MW (2014) Substitutional effects on structural and magnetotransport properties of La0.85-xSmxK0.15MnO3 (x = 0.05, 0.1 and 0.15). J Alloys Compd. 10:15–20. https://doi.org/10.1016/j.jallcom.2013.12.024

Wang WL, Meng Q, Weng X, Wu Z (2016) Rapid syntheses of ultrafine LaMnO3 nano-crystallites with superior activity for catalytic oxidation of toluene. Catal Commun. https://doi.org/10.1016/j.catcom.2016.06.030

Wang H, Lu Y, Han YX et al (2017) Enhanced catalytic toluene oxidation by interaction between copper oxide and manganese oxide in Cu–O–Mn/γ–Al2O3 catalysts. Appl Surf Sci. https://doi.org/10.1016/j.apsusc.2017.05.133

Wu J, Sun W, Cao L, Yang J (2016) Removal of highly concentrated toluene from flue gas by an anode-supported solid oxide fuel cell reactor to generate electricity. Chem Eng J. https://doi.org/10.1016/j.cej.2016.04.146

Zhang R, Li P, Xiao R et al (2016) Insight into the mechanism of catalytic combustion of acrylonitrile over Cu-doped perovskites by an experimental and theoretical study. Appl Catal B Environ. https://doi.org/10.1016/j.apcatb.2016.05.025

Zhu H, Zhang P, Dai S (2015) Recent advances of lanthanum-based perovskite oxides for catalysis. ACS Catal 5:6370–6385. https://doi.org/10.1021/acscatal.5b01667

Zonouz PR, Niaei A, Tarjomannejad A (2016) Modeling and optimization of toluene oxidation over perovskite-type nanocatalysts using a hybrid artificial neural network-genetic algorithm method. J Taiwan Inst Chem Eng. https://doi.org/10.1016/j.jtice.2016.05.020